Acta Mech 204, 155–173 (2009)
DOI 10.1007/s00707-008-0052-4

Anastasia H. Muliana · Sourabh Sawant

Responses of viscoelastic polymer composites with temperature and time dependent constituents

Received: 3 April 2008 / Revised: 27 May 2008 / Published online: 1 August 2008

Abstract This study formulates a concurrent micromechanical model for predicting effective responses of fiber reinforced polymer (FRP) composites, whose constituents exhibit thermo-viscoelastic behaviors. The studied FRP composite consists of orthotropic unidirectional fiber and isotropic matrix. The viscoelastic material properties for the fiber and matrix constituents are allowed to change with the temperature field. The composite microstructures are idealized with periodically distributed square fibers in a matrix medium. A unit-cell model, consisting of four fiber and matrix subcells, is generated to obtain effective nonlinear thermo-viscoelastic responses of the composites. A time-integration algorithm is formulated to link two different thermo-viscoelastic constitutive material models at the lowest level (homogeneous fiber and matrix constituents) to the effective material responses at the macro level, and to transfer external mechanical and thermal stimuli to the constituents. This forms a concurrent micromechanical model, which is needed as the material properties of the constituents depend on the temperature field. Consistent tangent stiffness matrices are formulated at the fiber and matrix constituents and also at the effective composite level to improve prediction accuracy. The thermo-viscoelastic responses obtained from the concurrent micromodel are verified with available experimental data. Detailed finite element (FE) models of the FRP microstructures are also generated using 3D continuum elements for several fiber volume fractions. Thermo-viscoelastic responses of the concurrent micromodel are also compared to the ones of the detailed FRP microstructures.

1 Introduction

Advanced polymer composites are designed to sustain extreme temperatures and mechanical loadings while remaining lightweight. Currently available fiber reinforced polymer (FRP) composites consist of synthetic (polymer) fibers, e.g., aramid, polyethylene, and high temperature polymer matrix, e.g., epoxy, polyamide. Under significant temperature changes and complex mechanical loadings, the properties of materials often vary with the temperature and deformation fields. Extreme temperatures and humid environments also intensify the viscoelastic behaviors of polymers. Experimental tests on aramid fibers and aramid FRP composites show that high temperatures decrease the strength and stiffness of the aramid fibers and aramid FRP [2,9,12,41,43]. Experimental tests on high temperature polyimide resin and polyimide reinforced composites also show that the elastic and viscoelastic response characteristics, strength, and thermal properties of polyimide systems are temperature dependent [4,6,13,21,35]. Under an extreme service environment, hygrothermal induced property deterioration is linked to chain scission of the polyimide cross links [21]. Current works on modeling

A. H. Muliana (✉) · S. Sawant
Department of Mechanical Engineering, Texas A&M University,
College Station, TX 77843-3123, USA
E-mail: amuliana@neo.tamu.edu
Tel.: +979-458-3579
Fax: +979-845-3081

temperature dependent viscoelastic responses have been extensively driven by the assumption of thermo-rheologically simple materials (TSM), in which the temperature effect is incorporated only through a time-scale shift factor [3,15,22]. This assumption is valid when the temperatures do not change the configuration of the polymer molecular (chemical) structures nor affect its elastic and long-term (relaxed) moduli [40,46]. When the polymer molecular structure significantly changes with temperature such that the elastic and relaxed moduli of the polymer depend upon the temperatures, the polymer is classified as a thermo-rheologically complex material (TCM) [5,40]. The time shifting technique has been extended to characterize a physical aging effect on the creep/relaxation responses of polymers with an assumption that the effect of the physical aging on the instantaneous elastic constant is not significant. Struik [39] has indicated that the material becomes stiffer during the physical aging process and the transient creep strain that carries the aging effect can be computed in the effective time-scale domain. Zheng and Weng [47] have shown that the physical aging effect must be accounted for in the case of long-term creep, while the physical aging effect is often negligible during short-term creep. They developed a constitutive model for predicting long-term creep for a class of materials whose long-term creep compliances can be constructed using the time-shifting technique on the logarithmic time scale.

It is well understood that reinforcement types, contents, and their distributions in the polymer matrix, together with the constituent properties, play important roles in determining the overall response of the composites. However, linking different viscoelastic behaviors of the fiber and matrix constituents, whose properties are also allowed to change with stress, strain, loading rates, moisture, and temperature fields, to the effective viscoelastic responses of the FRP composites is still lacking. Homogenization techniques have been widely developed to predict effective elastic and inelastic responses of composites, including viscoelasticity [1,7,17,18,32]. Micromechanical models with detailed spatial functions of the stress–strain fields give good response characteristics of the polymer composites; however, it is often difficult to obtain closed form solutions especially when material nonlinearity and complex loading are also involved. A simplified unit-cell model of a representative volume element (RVE), derived from periodically distributed microstructure, has been proposed to analyze fiber and particle reinforced composites [11,24,28]. The homogenization schemes are formulated in terms of the average constitutive relations in subcells within the unit-cell, which give approximated values of the overall composite behaviors. This method is computationally efficient and is suitable for incorporating nonlinear response and performing thermo-viscoelastic analyses of composite structures at multiple length-scales [26,25,31,30]. The above micromechanical models are derived to obtain effective viscoelastic composites having linear elastic inclusions (fibers or particles) and inelastic/viscoelastic matrix. In such case, the overall time-dependent behaviors of the composites are controlled by the matrix viscoelasticity.

To date, limited micromechanical models have been formulated to analyze thermo-viscoelastic behaviors of FRPs having different fiber and matrix viscoelasticity. Haddad and Tanari [8] proposed a microstructural model for temperature-dependent creep responses of composites having randomly oriented and short fibers. Both fiber and matrix exhibited linear viscoelastic behaviors. The time-dependent behavior of the individual fiber-bundle was formulated as a combination of a viscoelastic matrix substance within the bundle and an ensemble of unidirectional elastic fibers. Brinson and Knauss [5] used the correspondence principle of viscoelasticity to study the time–temperature behaviors of composite materials. Each phase in the composite system was modeled as TSM with linear viscoelastic and the resulting overall composite properties are TCM. A numerical model was presented to examine the TCM behaviors of the studied composite systems. Li and Weng [18] studied the influence of inclusion shape on thermomechanical properties of isotropic viscoelastic composites, i.e., cyclic stress–strain behavior cyclic creep master compliance curve, and effective thermal expansion coefficient. It is found that the viscoelastic properties of composites are strongly dependent upon the inclusion shape. It is also suggested that the creep compliance of composites with a thermo-rheologically simple matrix at various temperatures can all be plotted into a single master curve, via a reduced time scale. In other words, the composite also experiences TSM. Limited micromodel formulations that incorporate TCM characteristics of the matrix constituent have been developed. Hashin et al. [15] used a concentric cylinder assembly (CCA) to predict thermo-viscoelastic behaviors of unidirectional fiber composites having an elastic fiber and a TCM matrix system. Sadkin and Aboudi [36] and Aboudi [1] used the method of cell (MOC) to analyze thermal effects on the viscoelastic response of unidirectional fiber reinforced composites. The viscoelastic matrix was modeled as a TCM material. Recently, Muliana and Haj-Ali [31] derived micromechanical models for multi-layered composites with TCM characteristics of the polymer matrix. The fibers are assumed linearly elastic. The overall creep responses of the composites at different stresses and temperatures obtained from the micromodel are compared with experimental data of the multi-layered composites. Micromechanical modeling of heterogeneous materials having viscoelastic fiber and matrix constituents that follow TCM is still lacking.

This study formulates a concurrent micromechanical model for predicting effective viscoelastic behavior of FRP composites, whose fiber and matrix constituents exhibit different viscoelastic behavior. The viscoelastic responses of the unidirectional fibers and polymeric matrix are allowed to change with the temperature field and they are assumed to follow the TCM behavior. The formulations are suitable for small deformation gradient problems. The manuscript is organized as follows. Section 2 presents a time-dependent constitutive model for general orthotropic fiber materials having temperature dependent material properties. This constitutive model can be reduced to a linear elastic response in the case of carbon or glass fibers are considered; and it can be simplified to isotropic viscoelastic behaviors and used for the polymer matrix. Section 3 presents a unit-cell micromechanical model for the FRP. A time-integration algorithm with a stress correction scheme is formulated to link two different nonlinear time-dependent constitutive models of the fiber and matrix constituents to the overall composite viscoelastic responses. Numerical implementation and verification are discussed in Sect. 4. Available experimental data in the literature are used for comparisons. Furthermore, detailed FE models of the FRP microstructures are generated for several fiber volume fractions and the global responses obtained from the concurrent micromodel formulation are compared to the ones obtained from the detailed FE models.

2 Thermo-viscoelastic constitutive material models

This study uses the following constitutive relation for linearized thermo-viscoelastic behavior of solids (non-aging materials):

$$\varepsilon_{ij}^{t} \equiv \varepsilon_{ij}(t) = \int_0^t S_{ijkl}(T^{\tau}, (\psi^{t} - \psi^{\tau}))\frac{\partial \sigma_{kl}(\tau)}{\partial \tau}\mathrm{d}\tau + \int_0^t \alpha_{ij}(T^{\tau})\frac{\partial \Delta T(\tau)}{\partial \tau}\mathrm{d}\tau. \tag{1}$$

$\boldsymbol{S}$ is the creep compliance tensor that depends on the temperature field and α is the coefficient of linear thermal expansion (CTE) tensor that varies with temperature. At a reference temperature T_0, the material is under a stress-free condition and its properties are independent of temperature. The time and temperature dependent compliance for an orthotropic material is expressed as

$$S_{ijkl}(t, T) = S_{ijkl}(0, T) + \Delta S_{ijkl}(t, T), \tag{2}$$

where $\boldsymbol{S}(0, T)$ is the compliance at time 0, which is often considered as the time independent (instantaneous elastic) compliance, and $\boldsymbol{\Delta S}(t, T)$ is the transient time-dependent compliance. The temperature T can vary with time. Substituting Eq. (2) into (1) gives

$$\begin{aligned}\varepsilon_{ij}(t) &= \int_0^t \left[S_{ijkl}(0, T) + \Delta S_{ijkl}(t - \tau, T)\right]\frac{\mathrm{d}\sigma_{kl}(\tau)}{\mathrm{d}\tau}\mathrm{d}\tau + \int_0^t \alpha_{ij}(T^{\tau})\frac{\mathrm{d}\Delta T(\tau)}{\mathrm{d}\tau}\mathrm{d}\tau \\ &= S_{ijkl}(0, T)\sigma_{kl}(t) + \int_0^t \Delta S_{ijkl}(t - \tau, T)\frac{\mathrm{d}\sigma_{kl}(\tau)}{\mathrm{d}\tau}\mathrm{d}\tau + \int_0^t \alpha_{ij}(T^{\tau})\frac{\mathrm{d}\Delta T(\tau)}{\mathrm{d}\tau}\mathrm{d}\tau.\end{aligned} \tag{3}$$

Lou and Schapery [19] have extended the [38] nonlinear single integral form to characterize time-stress dependent behavior of orthotropic materials. In this study, the nonlinear material parameters are modeled as functions of the current temperature T^t. Thus, the creep function is expressed as

$$S_{ijkl}(t, T) = g(T^{\tau})S_{ijkl}(0, T) + f(T^{\tau})\Delta S_{ijkl}(t, T). \tag{4}$$

The transient compliance in Eq. (4) follows the Prony series exponential form, which is

$$\Delta S_{ijkl}^{\psi^t} = \sum_{n=1}^{N_{ijkl}} S_{ijkl}\left(1 - \exp\left[-\lambda_{ijkl}\psi^{t}\right]\right), \tag{5}$$

where N_{ijkl} is the number of terms for each component in the transient compliance tensor, $S_{ijkl(n)}$ is the nth coefficient of the Prony series for each component in the transient compliance tensor, and $\lambda_{ijkl(n)}$ is the nth

reciprocal of retardation time that corresponds to the $S_{ijkl(n)}$. The expression of the reduced time function ψ^t in Eq. (1) can be found in articles related to viscoelasticity, e.g., [46], which is

$$\psi^t \equiv \psi(t) = \int_0^t \frac{\mathrm{d}\xi}{a\left(T^\xi\right)}. \tag{6}$$

It is noted that in order for Eq. (1) be suitable for characterizing long-term material responses, it is necessary to include the physical aging effect, as stated in Zheng and Weng [47]. The above constitutive relation can be modified to include the physical aging effect by modifying the reduced time in Eq. (6), as suggested by Zheng and Weng [47]. For simplicity, the temperature dependent functions $g(T^t)$, $f(T^t)$ and $\mathrm{a}(T^t)$ are written as g^t, f^t and a^t, respectively, in the remainder of the manuscript. The superscript indicates the time-dependence of the variables. Substituting Eqs. (4) and (5) into Eq. (3) yields to the following mechanical strain:

$$\varepsilon_{ij}^{M,t} = g^t S_{ijkl}^0 \sigma_{kl}^t + f^t \sum_{n=1}^{N_{ijkl}} \left(S_{ijkl(n)} \sigma_{kl}^t\right) - f^t \sum_{k=1}^{3}\sum_{l=1}^{3}\sum_{n=1}^{N_{ijkl}} \underbrace{S_{ijkl(n)} q_{ijkl(n)}^t}_{\text{(no sum on i and j)}} \tag{7}$$

where

$$q_{ijkl(n)}^t = \int_0^t \exp\left[-\lambda_{ijkl(n)}(\psi^t - \psi^\tau)\right] \frac{\mathrm{d}\sigma_{kl}^\tau}{\mathrm{d}\tau} \mathrm{d}\tau \quad \text{(no sum on } k \text{ and l)}. \tag{8}$$

The integral form in Eq. (8) is solved recursively by dividing the integral into two parts. The first integral includes the limits $(0, t-\Delta t)$, i.e., up to the previous converged time step, which is stored as history variables. The limits of the second integral are taken as $(t-\Delta t, t)$, which is the current incremental time step. Detailed recursive iterative formulations can be found in [11] and [37]. By solving the integral form in Eq. (8) recursively, the scalar components of the incremental strain tensor at the current time t are defined by (see [37] for the detailed formulation)

$$\begin{aligned}\Delta\varepsilon_{ij}^{M,t} = &\left[\overline{S}_{ijkl}^t \sigma_{kl}^t - \overline{S}_{ijkl}^{t-\Delta t} \sigma_{kl}^{t-\Delta t}\right] + \sum_{k=1}^{3}\sum_{l=1}^{3}\sum_{n=1}^{N_{ijkl}} \underbrace{S_{ijkl(n)}\left(f^{t-\Delta t} - f^t \exp\left[-\lambda_{ijkl(n)}\Delta\psi^t\right]\right) q_{ijkl(n)}^t}_{\text{(no sum on } i \text{ and } j)} \\ &+ \sum_{n=1}^{N_{ijkl}} S_{ijkl(n)} \left[f^t \frac{1-\exp[-\lambda_{ijkl(n)}\Delta\psi^t]}{\lambda_{ijkl(n)}\Delta\psi^t} - f^{t-\Delta t} \frac{1-\exp[-\lambda_{ijkl(n)}\Delta\psi^{t-\Delta t}]}{\lambda_{ijkl(n)}\Delta\psi^{t-\Delta t}}\right] \sigma_{kl}^{t-\Delta t}.\end{aligned} \tag{9}$$

The nonlinear parameters in Eq. (9) are expressed as functions of the current temperature. The recursive numerical algorithm is designed to be compatible with the displacement based FE, in which the total strain and current incremental strain tensors are given as independent variables. For an uncoupled thermo-mechanical problem, the current temperature field at each incremental time step is also known. Using the constitutive model in Eq. (9), the current stresses are defined:

$$\begin{aligned}\sigma_{ij}^t = \overline{S}_{ijkl}^{t,-1} \Bigg\{ &\overline{S}_{ijkl}^{t-\Delta t} \sigma_{kl}^{t-\Delta t} + \Delta\varepsilon_{ij}^{M,t} - \sum_{k=1}^{3}\sum_{l=1}^{3}\sum_{n=1}^{N_{ijkl}} \underbrace{S_{ijkl(n)}\left(f^{t-\Delta t} - f^t \exp\left[-\lambda_{ijkl(n)}\Delta\psi^t\right]\right) q_{ijkl(n)}^t}_{\text{(no sum on } i \text{ and } j)} \\ &- \sum_{n=1}^{N_{ijkl}} S_{ijkl(n)} \left[f^t \frac{1-\exp[-\lambda_{ijkl(n)}\Delta\psi^t]}{\lambda_{ijkl(n)}\Delta\psi^t} - f^{t-\Delta t} \frac{1-\exp[-\lambda_{ijkl(n)}\Delta\psi^{t-\Delta t}]}{\lambda_{ijkl(n)}\Delta\psi^{t-\Delta t}}\right] \sigma_{kl}^{t-\Delta t} \Bigg\}.\end{aligned} \tag{10}$$

Finally, the consistent tangent stiffness matrix is determined by taking the inverse of the partial derivative of the incremental strain with respect to the incremental stress at the end of the current time step. The consistent tangent stiffness C^t_{ijkl}, at the converged state, is

$$C^t_{ijkl} \equiv \frac{\partial \Delta\sigma^t_{ij}}{\partial \Delta\varepsilon^{M,t}_{kl}} = \left[\frac{\partial \Delta\varepsilon^{M,t}_{ij}}{\partial \Delta\sigma^t_{kl}}\right]^{-1}. \tag{11}$$

The constitutive relation in Eq. (1) can be easily reduced to isotropic viscoelastic materials, which has been studied previously [11,29,37]. The incremental scalar components of the thermal strain are:

$$\begin{aligned} T^t &\equiv T^{t-\Delta t} + \Delta T^t, \\ \Delta\varepsilon^{T,t}_{ij} &\equiv \alpha(T^t)\Delta T^t \delta_{ij}. \end{aligned} \tag{12}$$

3 Micromechanical formulations

Extensive studies on the micromechanical formulations deal with combining a linear elastic fiber and a nonlinear viscoelastic matrix to obtain effective viscoelastic responses of FRP composites. In such case, the overall nonlinear and time-dependent characteristics of the composites depend mainly on the time-dependent function of the polymers. In this study, the previously developed unit-cell model of unidirectional FRP composites [11] is modified to incorporate different time-dependent functions for the compressible fiber and matrix constituents. The viscoelastic and thermal properties of the fiber and matrix constituents are also allowed to change with the temperature field. Thus, the overall composite responses are time and temperature dependent. It is also possible to incorporate stress, strain, strain rate and moisture dependent parameters in the micromodel formulation. However, these are not the scope of this paper. It is assumed that the effects of volume changes in the fiber and matrix constituents during time-dependent deformation on the overall viscoelastic responses of the FRP are negligible. In other words, the fiber volume content during the deformation remains constant. Two-way micromechanical relations that provide effective composite behaviors by homogenizing properties of the fiber and matrix constituents, and simultaneously transfer the external mechanical and thermal stimuli to the fiber and matrix constituents are formulated.

A simplified micromechanical relation is derived from the idealized FRP microstructures, which are modeled as periodic distributed arrays of square fibers embedded in a polymeric matrix (Fig. 1). A composite RVE

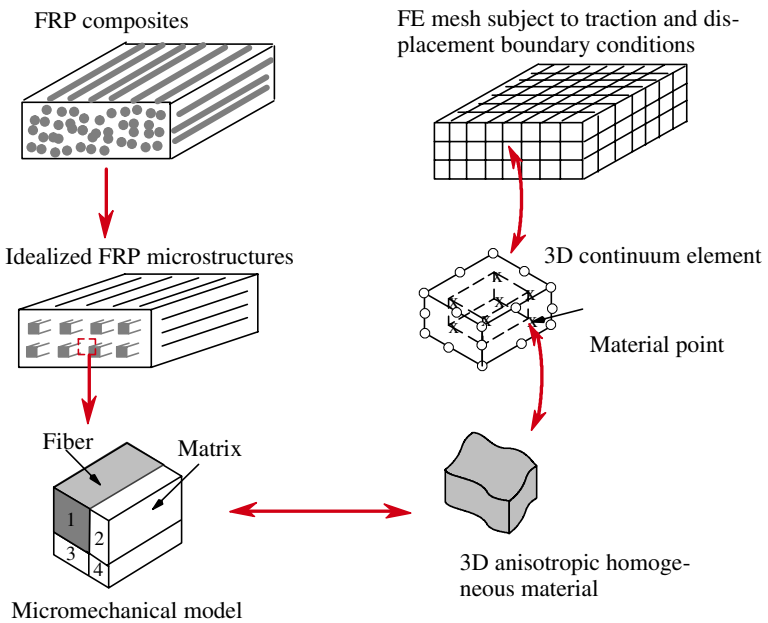

Fig. 1 Idealized micromechancial model for fiber reinforced polymers

is defined by a square fiber placed in the center of a square matrix domain. A one fourth unit-cell micromechanical model consisting of four subcells is generated due to the two-plane symmetry in the RVE. The viscoelastic constitutive relations with temperature dependent material parameters are examined at the fiber and matrix subcells. The micromechanical relations are formulated by assuming a perfect bond between the interphase fiber and matrix. The result from the micromechanical relations is a 3D effective anisotropic viscoelastic response of a homogenous composite medium. The current micromechanical model derived from periodic unit-cell models is designed to be suitable for FE structural analyses of thermo-viscoelastic responses. The 3D effective anisotropic response is implemented at every material point in a FE mesh. It is also necessary to determine stress, strain and temperature fields in the fiber and matrix subcells from the external thermal and mechanical stimuli applied at the composites (global structural level). This is achieved by formulating concentration matrices that relate the composite effective field quantities to the constituent field quantities. The advantage of using the current micromechanical approach is that it allows determining thermal stresses in each subcell (constituent) due to the mismatch in the coefficients of thermal expansion between the fiber and matrix constituents. The existence of thermal stresses in the constituents can significantly influence the overall responses of composites.

The nonlinear and time-dependent responses are solved in an iterative manner with linearized incremental stress–strain relation and iterative correction schemes within an incremental time step. Stress correction scheme is performed in the unit-cell (micromechanical) model. This is done in order to minimize the residual due to the linearization. At every incremental time step, the concentration matrices are formulated and the consistent tangent stiffness of the fiber, matrix, and composites are updated once convergence is achieved.

3.1 Linearized micromechanical relations

At the current time t, the total effective stresses and strains are given as

$$\begin{aligned} \overline{\sigma}_{ij}^{t} &\equiv \overline{\sigma}_{ij}^{t-\Delta t} + \Delta\overline{\sigma}_{ij}^{t}, \\ \overline{\varepsilon}_{ij}^{t} &\equiv \overline{\varepsilon}_{ij}^{t-\Delta t} + \Delta\overline{\varepsilon}_{ij}^{t}. \end{aligned} \tag{13}$$

The superscript $t-\Delta t$ denotes the field quantities from the previous converged step, which are stored as history variables. A basic unit-cell that represents geometrical and material characteristics is defined. The unit-cell is divided into a number of subcells and the spatial variation of the displacement field in each subcell is assumed such that the stresses and deformations are spatially uniform. Traction continuity and displacement compatibility at an interface between subcells are satisfied in an average sense. Thus, the incremental average stresses and strains in the unit-cell model at time t are defined by:

$$\Delta\overline{\sigma}_{ij}^{t} \equiv \frac{1}{V}\sum_{\alpha=1}^{N}\int_{V^{(\alpha)}} \Delta\sigma_{ij}^{t,(\alpha)}(x_k^{(\alpha)})\mathrm{d}V^{(\alpha)} \approx \frac{1}{V}\sum_{\alpha=1}^{N} V^{(\alpha)}\Delta\sigma_{ij}^{t,(\alpha)}, \tag{14}$$

$$\Delta\overline{\varepsilon}_{ij}^{t} \equiv \frac{1}{V}\sum_{\alpha=1}^{N}\int_{V^{(\alpha)}} \Delta\varepsilon_{ij}^{t,(\alpha)}(x_k^{(\alpha)})\mathrm{d}V^{(\alpha)} \approx \frac{1}{V}\sum_{\alpha=1}^{N} V^{(\alpha)}\Delta\varepsilon_{ij}^{t,(\alpha)}. \tag{15}$$

The superscript denotes the subcells number and N is the number of subcells. The stress $\Delta\sigma_{ij}^{(\alpha)}$ and strain $\Delta\varepsilon_{ij}^{(\alpha)}$ are the incremental average stress and strain within each subcell. The unit-cell volume V is $V = \sum_{\alpha=1}^{N} V^{(\alpha)}$.

Detailed micromechanical stress and strain relations within the subcells for the unidirectional FRP can be found in [11,24], which are summarized in Appendix A. Next, concentration matrices that relate the global average (macro) quantities to the local (micro) quantities are formulated. A stress-concentration matrix is formulated when the stresses are prescribed at the macro level. When the macrostrains are given, a strain-concentration matrix is defined. In this study, the micromechanical model is designed to be compatible with displacement based FE structural analyses, in which the effective incremental strain $\Delta\overline{\varepsilon}^{t}$ is chosen as the independent tensor. Thus, the subcell strain-interaction matrix ($B^{t,(\alpha)}$), which relates the subcell average strains, $\Delta\varepsilon^{t,(\alpha)}$, to the unit-cell average strain, $\Delta\overline{\varepsilon}^{t}$, is:

$$\Delta\varepsilon_{ij}^{t,(\alpha)} = B_{ijkl}^{t,(\alpha)}\Delta\overline{\varepsilon}_{kl}^{t}. \tag{16}$$

Substituting Eq. (16) into (15) gives

$$\Delta\overline{\varepsilon}_{ij}^{t} = \frac{1}{V}\sum_{\alpha=1}^{N} V^{(\alpha)} B_{ijkl}^{t,(\alpha)} \Delta\overline{\varepsilon}_{kl}^{t}. \tag{17}$$

Equation (17) must hold for an arbitrary average strain $\Delta\overline{\varepsilon}^{t}$, which requires the following relations to be satisfied:

$$\frac{1}{V}\sum_{\alpha=1}^{N} V^{(\alpha)} B_{ijkl}^{t,(\alpha)} = \delta_{ik}\delta_{jl}. \tag{18}$$

Using the strains defined in Eq. (16), the constitutive equation for linearized stress–strain relations in each subcell is expressed as

$$\Delta\sigma_{ij}^{t,(\alpha)} = C_{ijkl}^{t,(\alpha)} \Delta\varepsilon_{kl}^{t,(\alpha)} = C_{ijkl}^{t,(\alpha)} B_{klrs}^{t,(\alpha)} \Delta\overline{\varepsilon}_{rs}^{t}, \tag{19}$$

where $C^{t,(\alpha)}$ is the consistent tangent stiffness matrix of the subcell (α), which is defined in Eq. (11). Substituting Eqs. (19) into (14) gives:

$$\Delta\overline{\sigma}_{ij}^{t} = \frac{1}{V}\sum_{\alpha=1}^{N} V^{(\alpha)} C_{ijkl}^{t,(\alpha)} B_{klrs}^{t,(\alpha)} \Delta\overline{\varepsilon}_{rs}^{t}. \tag{20}$$

The unit-cell effective tangent stiffness matrix $\overline{C}^{t}$ is determined by

$$C_{ijrs}^{t} = \frac{1}{V}\sum_{\alpha=1}^{N} V^{(\alpha)} \overline{C}_{ijkl}^{t,(\alpha)} B_{klrs}^{t,(\alpha)}. \tag{21}$$

It is also possible to define a stress interaction matrix $F^{(\alpha)}$, which relates the subcell average stress, $\Delta\sigma^{t,(\alpha)}$, to the unit-cell average stress, $\Delta\overline{\sigma}^{t}$:

$$\Delta\sigma_{ij}^{t,(\alpha)} = F_{ijkl}^{t,(\alpha)} \Delta\overline{\sigma}_{kl}^{t}. \tag{22}$$

Using the constitutive equation for each subcell, the incremental strains in each subcell can be determined:

$$\Delta\varepsilon_{ij}^{t,(\alpha)} = \left[C_{ijkl}^{t,(\alpha)}\right]^{-1} F_{klmn}^{t,(\alpha)} \Delta\overline{\sigma}_{mn}^{t}. \tag{23}$$

Substituting Eqs. (23) into (15) gives

$$\Delta\varepsilon_{ij}^{t,(\alpha)} = \frac{1}{V}\sum_{\alpha=1}^{N} V^{(\alpha)} \left[C_{ijkl}^{t,(\alpha)}\right]^{-1} F_{klmn}^{t,(\alpha)} \Delta\overline{\sigma}_{mn}^{t}. \tag{24}$$

Finally, the unit-cell effective tangent stiffness matrix $\overline{C}^{t}$ is determined by

$$[\overline{C}_{ijmn}^{t}]^{-1} = \sum_{\alpha=1}^{N} V^{(\alpha)} [C_{ijkl}^{t,(\alpha)}]^{-1} F_{klmn}^{t,(\alpha)}. \tag{25}$$

Furthermore, the RVEs length scale is assumed to be much smaller than the macrostructural scale such that the steady state condition in each unit-cell (represented by a material point) is reached in a very short period in comparison to the overall time responses. Therefore, the transient heat conduction analysis in each unit-cell of the RVE is bypassed and temperatures are assumed to vary only within the global material points. The total temperature in each unit-cell at the steady-state condition is defined by

$$\begin{aligned} \Delta T^{t,(\alpha)} &= \Delta\overline{T}^{t}, \\ T^{t+\Delta t,\alpha} &= T^{t,(\alpha)} + \Delta T^{t,(\alpha)}. \end{aligned} \tag{26}$$

In the case of temperature boundary conditions being considered, the micromechanical relations in Appendix A are defined in terms of total mechanical and thermal quantities. This allows calculating thermal stresses due to the mismatch in the coefficients of thermal expansion of the fiber and matrix constituents.

3.2 Formulation of the $\boldsymbol{B}$ matrices

Up to this point, the strain-interaction matrices $\boldsymbol{B}^{t,(\alpha)}$ or the stress-interaction matrices $\boldsymbol{F}^{t,(\alpha)}$ have not been determined. In order to derive the strain-interaction matrices or the stress-interaction matrices for all subcells, the micromechanical relations together with the subcells' constitutive material models are used. In the case that $\boldsymbol{B}^{t,(\alpha)}$ matrices are formulated, six components of strains need to be determined in every subcell. Thus, a total of 24 strain components are defined, which requires forming 24 equations. The first set of equations is formulated from the strain compatibility equations, which are

$$\left\{\boldsymbol{R}_{\varepsilon}^{t}\right\} = [\boldsymbol{A}_1] \begin{Bmatrix} \Delta\varepsilon^{t,(1)} \\ \Delta\varepsilon^{t,(2)} \\ \Delta\varepsilon^{t,(3)} \\ \Delta\varepsilon^{t,(4)} \end{Bmatrix} - [\boldsymbol{D}] \left\{\Delta\overline{\varepsilon}^{t}\right\}, \tag{27}$$

where $\boldsymbol{R}_{\varepsilon}^{t}$ is the residual vector arising from imposing linearized strain compatibility relations with nonlinear constitutive relations in all subcells. In the case of linear elastic responses assumed in all subcells, the vector $\boldsymbol{R}_{\varepsilon}^{t}$ is automatically reduced to zero. The components of the matrices $\boldsymbol{A}_1$ and $\boldsymbol{D}_1$ in Eq. (27) are given in Appendix B. The second set of equations is formed by satisfying the traction continuity relations. Up to this stage, the components of the effective stress tensor $\overline{\sigma}_{ij}^{t}$ remain unknown. Equations based on the traction continuity relations within subcells should avoid the presence of $\overline{\sigma}_{ij}^{t}$, which are written as

$$\left\{\boldsymbol{R}_{\sigma}^{t}\right\} = \left[\boldsymbol{A}_2^{t}\right] \begin{Bmatrix} \Delta\varepsilon^{t,(1)} \\ \Delta\varepsilon^{t,(2)} \\ \Delta\varepsilon^{t,(3)} \\ \Delta\varepsilon^{t,(4)} \end{Bmatrix} - [\boldsymbol{O}] \left\{\Delta\overline{\varepsilon}^{t}\right\}. \tag{28}$$

The residual vector $\boldsymbol{R}_{\sigma}^{t}$ is due to the traction continuity relations, which for linear elastic constituents of its components are zero. The matrix $\boldsymbol{O}$ is the zero matrix. The matrices $\boldsymbol{B}^{t,(\alpha)}$ in Eq. (16) are then formed using Eqs. (27) and (28), which in linearized relations yields

$$\begin{bmatrix} \boldsymbol{B}^{t,(1)} \\ \cdots \\ \boldsymbol{B}^{t,(4)} \end{bmatrix} = \begin{bmatrix} \boldsymbol{A}_1 \\ \boldsymbol{A}_2^{t} \end{bmatrix}^{-1} \begin{bmatrix} D \\ O \end{bmatrix}. \tag{29}$$

Once the matrices $\boldsymbol{B}^{t,(\alpha)}$ are determined, the strain components in each subcell is also known and the nonlinear constitutive relations in each subcell can be calculated. Finally, the effective homogenized stresses and tangent stiffness matrix are solved using Eqs. (20) and (21), respectively.

3.3 Iterative correction schemes

The linearized micromechanical relations will give exact solutions when the constitutive material models for all subcells are linear elastic. In this study, the fiber and matrix subcells experience different nonlinear and time-dependent behaviors, in which upon imposing the micromechanical relations in Appendix A leads to nonzero residual strain and stress as defined in Eqs. (27) and (28). An iterative corrector scheme is formulated at every incremental time step to satisfy both the micromechanical constraints and the nonlinear viscoelastic constitutive equations. The residual vector is defined using Eqs. (27) and (28) in the case of components of the effective strain chosen as independent variables, which is presented in this study. To minimize the 24 components of the residual vector, the subcells' stress–strain components need to be corrected, which involves a total of 48 stress and strain scalar variables in the four subcells. These scalar variables are related via constitutive relations leading to only 24 independent variables. In this study, the components of strains in each subcell $\varepsilon_{ij}^{(\alpha)}$ are chosen as independent variables, which are:

$$X^{t,T} = \left\{ \varepsilon^{t,(1)} \;\; \varepsilon^{t,(2)} \;\; \varepsilon^{t,(3)} \;\; \varepsilon^{t,(4)} \right\}. \tag{30}$$

The stress components in the subcells are defined as functions of independent variables X_{ij}^t. The Newton Raphson (NR) iterative method is used to minimize the residual vector and find the solutions of variables X_{ij}^t:

$$X_{ij}^{t,k+1} = X_{ij}^{t,k} + \left[\frac{\partial \boldsymbol{R}_{ij}^{t,k}}{\partial X_{kl}}\right] \boldsymbol{R}_{kl}^{t,k}. \tag{31}$$

A converged solution is achieved when the residual vectors $\boldsymbol{R}_{\varepsilon}^t$ and $\boldsymbol{R}_{\sigma}^t$ are diminished. Once convergence is achieve, the current incremental stresses and consistent tangent stiffness matrix in Eqs. (20) and (21), respectively, are updated.

4 Numerical implementation and verification

The thermo-viscoelastic responses obtained from the micromechanical model are first verified using limited experimental data on unidirectional FRP composites of carbon-polyimide and Kevlar-epoxy systems. Elastic material properties of the carbon-polyimide composites with 56% volume fractions at various temperatures are obtained from Kumosa and collaborators [4,33,35]. Creep compliances of Kevlar-epoxy systems having 63% volume fraction studied by Walruth [41] are also used to verify the micromodel prediction of the overall time-dependent responses. Furthermore, detailed FE meshes of composite's RVEs at several fiber volume fractions (20, 40 and 50%) are generated. Thermo-viscoelastic responses from the micromodel formulation are compared to the ones obtained using the detailed FRP meshes.

4.1 Temperature dependent elastic properties of graphite T360/PMR-15 polyimide systems

The micromechanical model is used to determine the effective elastic stiffness of carbon-polyimide composites with 56% volume fraction. The in situ elastic properties for the transversely isotropic carbon fiber and isotropic polyimide matrix measured at room temperature are given in Table 1. The temperature dependent elastic modulus for the polyimide system, reported by [35], is illustrated in Fig. 2. Within the studied temperature range the elastic properties of the carbon fiber is assumed independent of temperature. The temperature

Table 1 Elastic material properties for T300 Graphite and PMR-15 matrix

	E_{11} (GPa, ksi)	$E_{22} = E_{33}$ (GPa, ksi)	$G_{12} = G_{13}$ (GPa, ksi)	G_{23} (GPa, ksi)	$\nu_{12} = \nu_{13}$ (GPa, ksi)	ν_{23} (GPa, ksi)
Fiber (T650-35-graphite)	224 (32,480)	15.4 (2,233)	21.1 (3,060)	5.8 (841)	0.40	0.40
Matrix (PMR15-polyimide)	3.97 (576)				0.36	

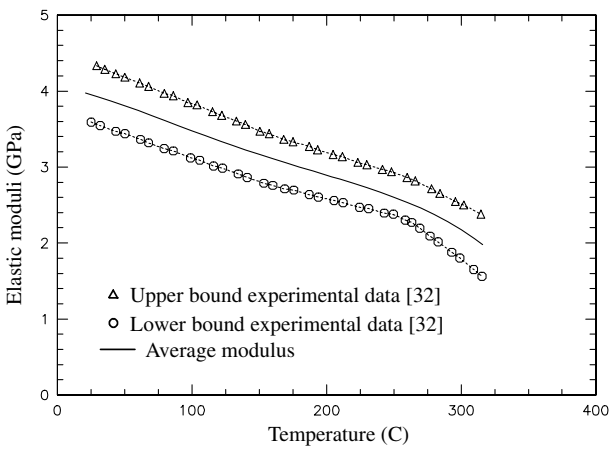

Fig. 2 Temperature dependent elastic modulus of polyimide matrix

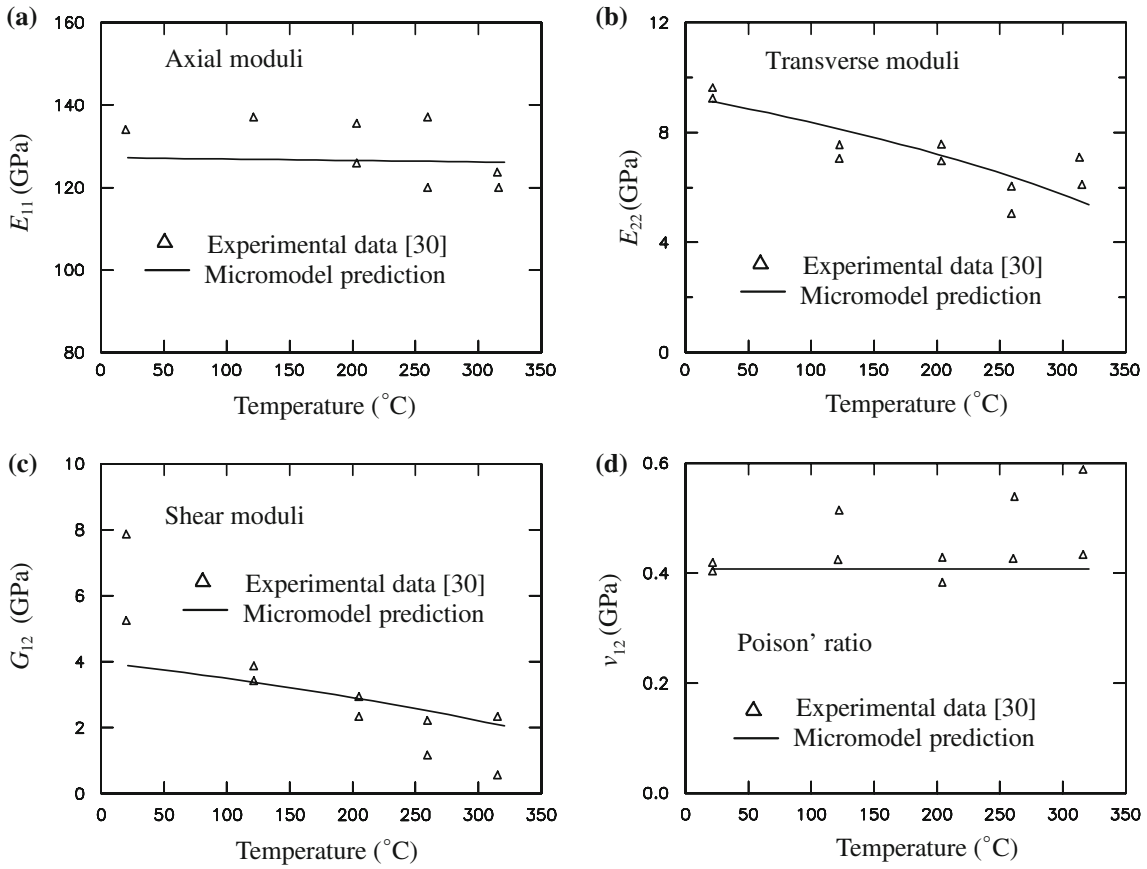

Fig. 3 Micromodel predictions of temperature-dependent elastic properties of carbon-polyimide systems with 56% volume fraction

Table 2 Elastic properties for Kevlar-49 fiber and epoxy-3501 matrix

	E_{11} (GPa)	$E_{22} = E_{33}$ (GPa)	$G_{12} = G_{13}$ (GPa)	G_{23} (GPa)	$\nu_{12} = \nu_{13}$ (GPa)	ν_{23} (GPa)
Fiber (Kevlar-49)	113–129	6	4.14	3.3	0.40	0.40
Matrix (epoxy-3501)	4.34				0.36	

dependent elastic moduli for the polyimide matrix are calibrated using the average values in Fig. 2. The fitted function in terms of the temperature-dependent elastic compliance, as shown in Eq. (4), is given as:

$$g(T) = 5.59 \times 10^{-8} T^3 - 1.97 \times 10^{-5} T^2 + 4 \times 10^{-3} T + 0.9, \quad T \text{ in}^\circ\text{C}. \tag{32}$$

Figure 3 depicts micromodel predictions of the elastic properties of graphite/PMR-15 polyimide unidirectional composites at different temperatures. The elastic moduli of the polyimide are allowed to degrade as the temperature increases, while the fiber moduli remain constant within the studied temperature range. Overall, good predictions are observed.

4.2 Time-dependent responses of Kevlar-49/epoxy composites

The effective time-dependent responses of FRP composites obtained from the micromechanical model is verified using experimental data of Kevlar-49/epoxy 3501 (KFRP) composites with 63% fiber volume fraction reported by Walruth [41]. The Kevlar fiber and epoxy matrix have different time-dependent material responses. Since the reported data in Walruth [41] are for the effective KFRP composites, as inputs to the micromechanical model we use existing data of the viscoelastic properties of Kevlar-49 and epoxy-3501. The elastic properties for the Kevlar fiber and the epoxy matrix are given in Table 2. A wide variation in axial moduli of the Kevlar-49

Table 3 Effective elastic properties for KFRP composites with 63% volume fraction

	E_{11} (GPa)	$E_{22} = E_{33}$ (GPa)	$G_{12} = G_{13}$ (GPa)	G_{23} (GPa)	$\nu_{12} = \nu_{13}$ (GPa)
Micromodel	78.1	5.61	2.86	2.65	0.385
Experiment	77.9	5.60	2.20	1.90	0.4

Experimental data is obtained from Walruth [41]

Table 4 Prony parameters for unidirectional Kevlar-49 and epoxy 3501

n	λ_n(min^{-1})	$D_n \times 10^{-6}$(MPa^{-1})		
		Kevlar (S_{1111})	Kevlar (S_{2222})	Epoxy
1	1	0.73	0.07	176
2	10^{-1}	0.071	0.1	5
3	10^{-2}	0.31	2.8	29
4	10^{-3}	0.03	0.44	25
5	10^{-4}	0.48	4.2	35
6	10^{-5}	0.38	0.4	6.8

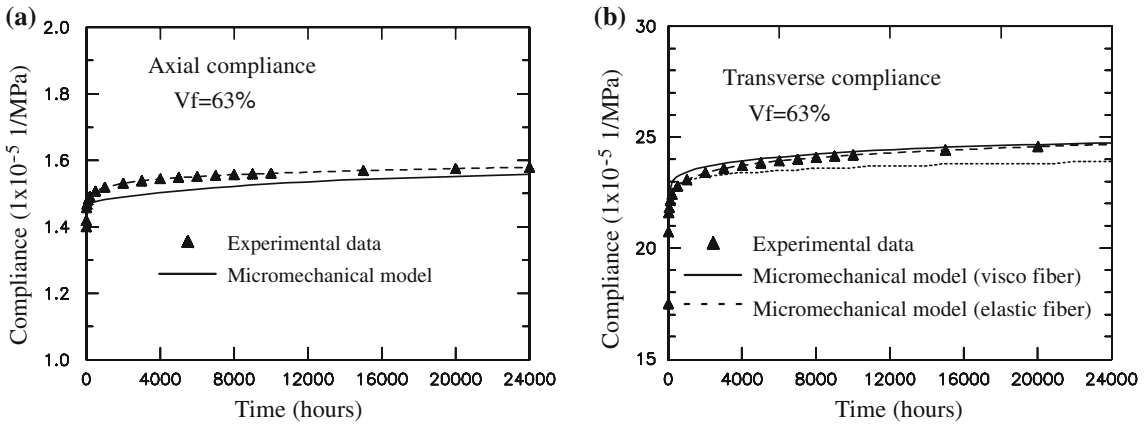

Fig. 4 Effective compliances for Kevlar-49/epoxy-3501 composites

fibers between 113 and 129 GPa is observed in the existing literature [42,44]. The axial modulus of the fiber can significantly affect the effective elastic modulus of the composite along the axial fiber direction. The proposed micromechanical model is used to obtain effective elastic material properties of the KFRP composites. The axial modulus of the Kevlar-49 is taken as 121 GPa, which is the average value of the upper and lower moduli. The predictions of the effective elastic properties are in good agreement with the ones reported by Walruth [41], which are shown in Table 3. The Kevlar fiber exhibits a transversely isotropic linear viscoelastic response, while the matrix experiences an isotropic viscoelastic response. The creep compliance for the Kevlar-49 fiber in the longitudinal fiber direction is obtained from [42]. The creep compliance for epoxy-3501 resin is obtained from [45]. Prony parameters are used to fit the creep compliances, which are given in Table 4. The axial fiber direction follows a time-dependent response, while along the transverse direction an elastic behavior is assumed. The effective creep compliance in the axial and transverse directions for the KFRP composites is illustrated in Fig. 4. The micromechanical model shows good prediction capabilities in the axial fiber direction. A slight mismatch is found in the transverse compliance due to the assumption of a linear elastic transverse modulus of Kevlar fibers. As experimental data on the viscoelastic properties of Kevlar in the transverse fiber direction are not available, we calibrated the time-dependent transverse compliance of the fibers by changing the time-dependent parameters in the compliance $S_{2222}(t)$ for Kevlar until the overall responses from the micromodel matched the ones from the experiments. The calibrated $S_{2222}(t)$ is shown in Table 4.

Furthermore, to verify the micromechanical creep responses of KFRP composites at different fiber volume fractions, i.e., 20, 40 and 50%, detailed FE meshes of the composite microstructures are generated. Two unit-cell model of the FRP microstructures are considered, as shown in Fig. 5. The first unit-cell consists of one-fourth symmetry of one cylindrical fiber embedded in a matrix of a rectangular solid. The second

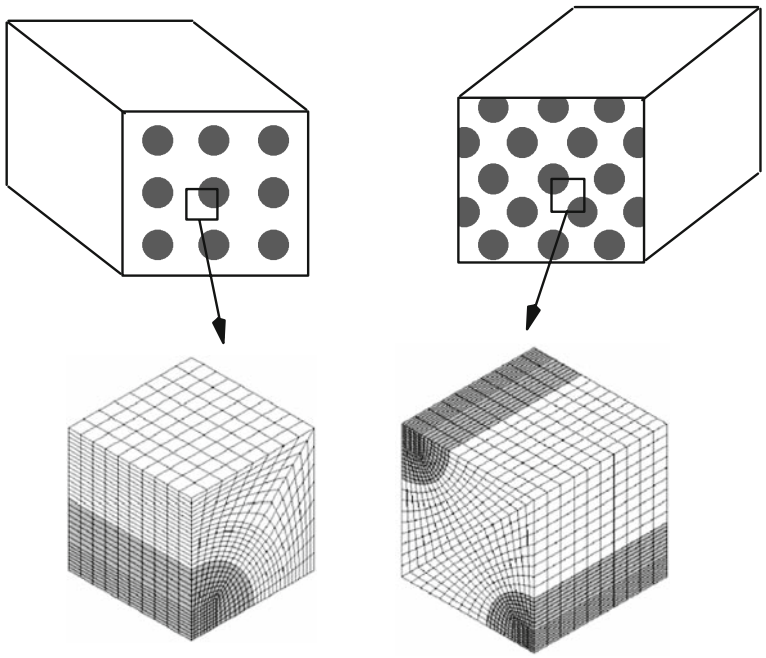

Fig. 5 FE model for unidirectional FRP microstructures (idealized microstructures, vf = 20%)

unit-cell consists of two one-quarter fibers placed in a matrix of a rectangular solid. Figure 5 also shows detailed FE models of the idealized FRP microstructures using 3D continuum (C3D8) elements. Material parameters for the Kevlar fiber and epoxy matrix are given in Tables 2 and 4. The recursive integration algorithm for nonlinear viscoelastic materials are implemented at each material (Gaussian) points in the finite elements. Creep responses of the composites along the axial and transverse fiber directions, which are determined at fixed temperatures, are illustrated in Fig. 6. The axial creep responses obtained from the concurrent micromechanical model match very well with the ones generated using the detailed FE microstructures having single and two fibers. The transverse creep compliances generated using the concurrent micromodel are in good correlations with the detailed FE micromodel with single fiber inclusion. Slight mismatches are shown in the transverse compliances generated using the concurrent micromodel and detailed FE microstructures with two fibers for higher volume fractions. The deviations are between 5.5 and 8.5%. In the two-fiber FE unit-cell model, as the fiber volume content increases the distant between the two fibers (spacing) is smaller and the transverse loading creates high localized stresses around the fiber spacing. This might be due to the fiber interactions, as shown in Fig. 7. It is seen that for composites with 50% fiber volume fraction, the stress gradient in the fiber constituents in the two-fiber model is higher compared to the one in the single fiber model. In the single fiber model, a relatively uniform stress is observed in the fiber constituents. The concurrent micromechanical model relations are formulated in terms of average stress tensor in the fiber subcell and do not incorporate stress variations in the fibers.

The stress–strain behavior of the KFRP/epoxy composites at various constant stress rates is also presented. Responses from the micromechanical model are compared to the ones obtained from the detailed FE microstructures having a single fiber for composites with 20, 40 and 50% volume fractions. Three different stress rates: 0.01, 0.1, and 0.5 MPa/h are considered. Figure 8 presents stress–strain responses due to loading in the transverse fiber direction. The micromodel predictions of the stress–strain responses at different loading rates are comparable to the responses from the FE model of the FRP microstructures. The concurrent micromechanical model is capable of modeling the effective responses of the FRP composites at different loading rates.

4.3 Effective viscoelastic responses of composites subject to mechanical and thermal stimuli

The capability of the concurrent micromechanical model in incorporating different time-dependent behaviors of the constituents at various temperatures is presented. The studied FRP systems consist of Kevlar fibers

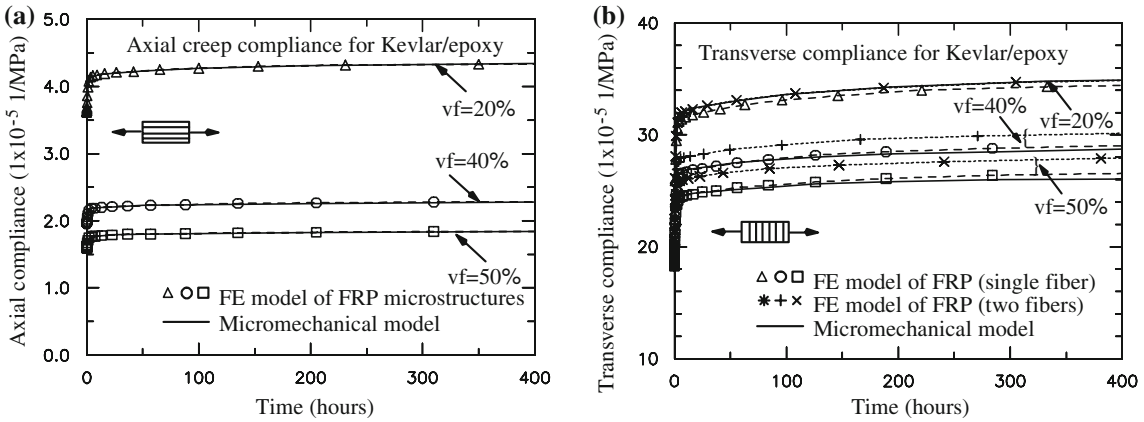

Fig. 6 Axial and transverse creep compliances of KFRP composites at 20, 40, and 50% volume fractions

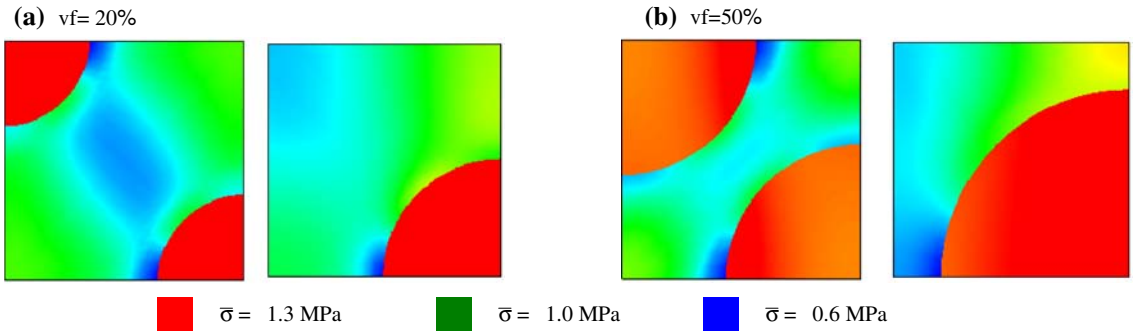

Fig. 7 Comparisons of the Von Mises stress contour of FRP microstructures with 20 and 50% volume fractions (results from detailed FE model)

and a PMR-15 polyimide matrix, which exhibit different time-dependent properties. Hanson [12] has studied the feasibility of a Kevlar-49/PMR-15 composite for high temperature aerospace structures. It was observed that polyimide resin PMR-15 provides thermo-oxidative and hydrothermal stability even at relatively high temperatures. A significant reduction in baseline flexural modulus and strength was observed with increase in temperature from 25 to 316°C. Degradation in the FRP modulus was also observed during a long-term exposure (1,500 h) at 285°C. In this study, time-dependent material properties for the Kevlar fibers, given in Table 4, are used, while the viscoelastic responses of the PMR-15 are taken from [20]. Marias and Villoutreix [20] have characterized 5 h creep behavior of PMR-15 at several isothermal temperatures (250–300°C). Experimental creep responses of the PMR-15 polyimide at temperatures of 250, 275, 285 and 300°C are illustrated in Fig. 9. The elastic properties of the PMR-15 at room temperature are $E = 3{,}625$ MPa and $\nu = 0.3$ and the time-dependent properties of the PMR-15 are given in Table 5. The temperature-dependent parameters for the PMR-15 are:

$$\begin{aligned} g_0(T) &= 5.59 \times 10^{-8} T^3 - 1.97 \times 10^{-5} T^2 + 4.01 \times 10^{-3} T + 0.9, \quad T \text{ in}^\circ\text{C}, \\ f(T) &= 3.116 \times 10^{-5} T^3 + 2.777 \times 10^{-2} T^2 - 8.1196 T + 782.01, \\ a(T) &= 1.333 \times 10^{-5} T^3 - 1.1 \times 10^{-2} T^2 + 3.0087 T - 272. \end{aligned} \tag{33}$$

Instead of recalibrating the parameter $g(T)$, which describes the variation of the elastic modulus of PMR-15 with temperature, the previously calibrated $g(T)$ parameter in Eq. (32) from [35] is used. This is done to evaluate the consistency of the temperature-dependent material parameters obtained from different sets of experimental data. To calibrate temperature-dependent parameters $f(T)$ and $a(T)$, first attempt is to use only the time–temperature shifting parameter $a(T)$ for representing experimental creep responses at various temperatures reported in [20]. This describes the thermo-rheologically simple behaviors. However, using only the parameter $a(T)$ does not provide a good fit in representing creep responses at higher temperatures (285 and 300°C). The second attempt is to include the temperature dependent parameters $g(T)$ and $f(T)$. A good

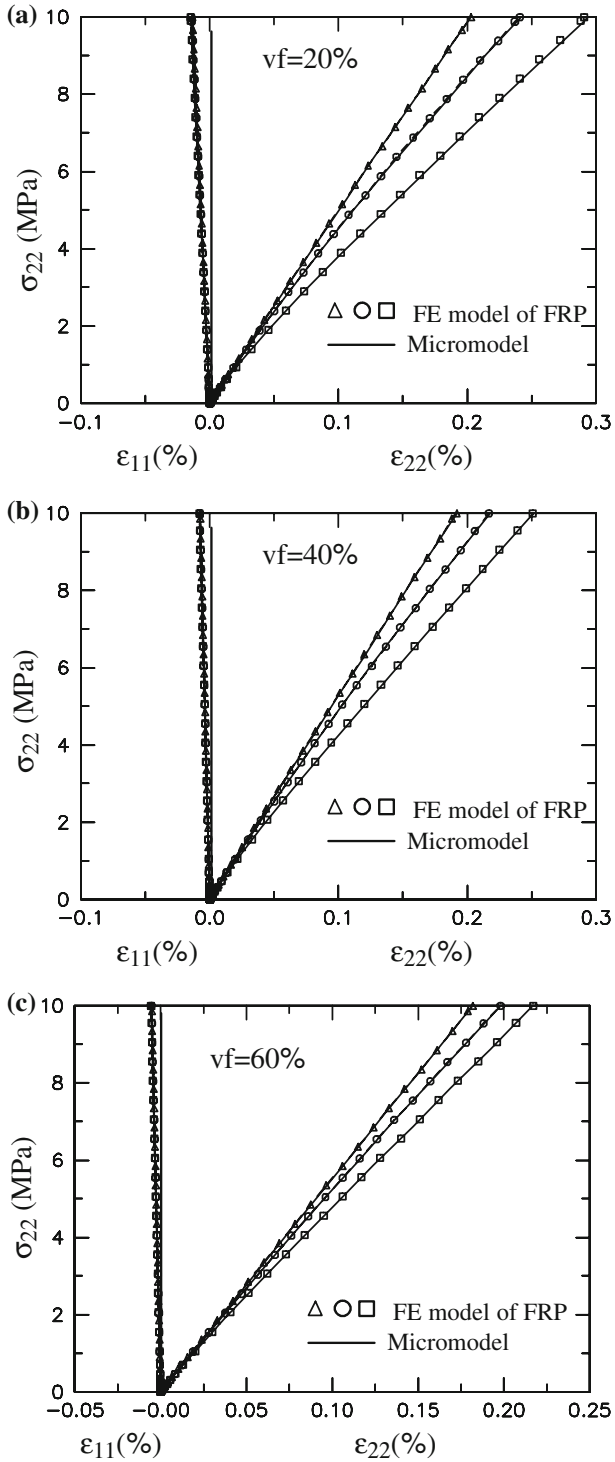

Fig. 8 Stress–strain behaviors of Kevlar/epoxy composites at various constant stress rates (*triangles* $r = 0.5$ MPa/h, *circle* $r = 0.1$ MPa/h, *squares* $r = 0.01$ MPa/h)

fit to experimental data is achieved even at high temperatures. The capability of the time-integration algorithm presented in Eqs. (7) and (11) in predicting creep responses at various temperatures is illustrated in Fig. 9. Good response predictions are shown.

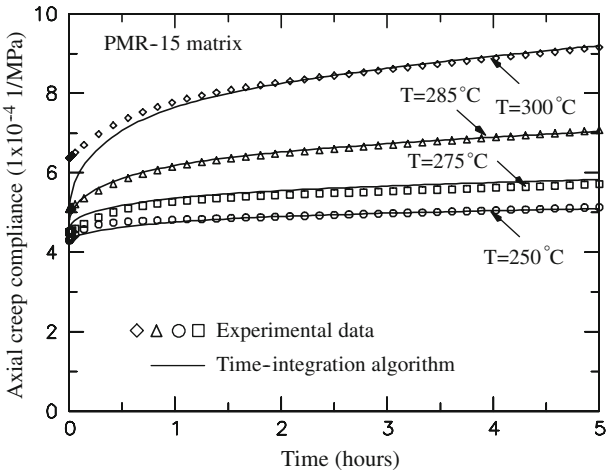

Fig. 9 Creep compliance for PMR-15 matrix at various temperatures

Table 5 Time-dependent properties for PMR-15 (calibrated from experimental data in [20])

n	$\lambda_n(\mathrm{h}^{-1})$	$D_n \times 10^{-6}(\mathrm{MPa}^{-1})$
1	30	7.5
2	10	7.0
3	2	20.0
4	1	10.0
5	0.5	2.0
6	0.1	19.0
7	0.01	190.0
8	0.001	850.0

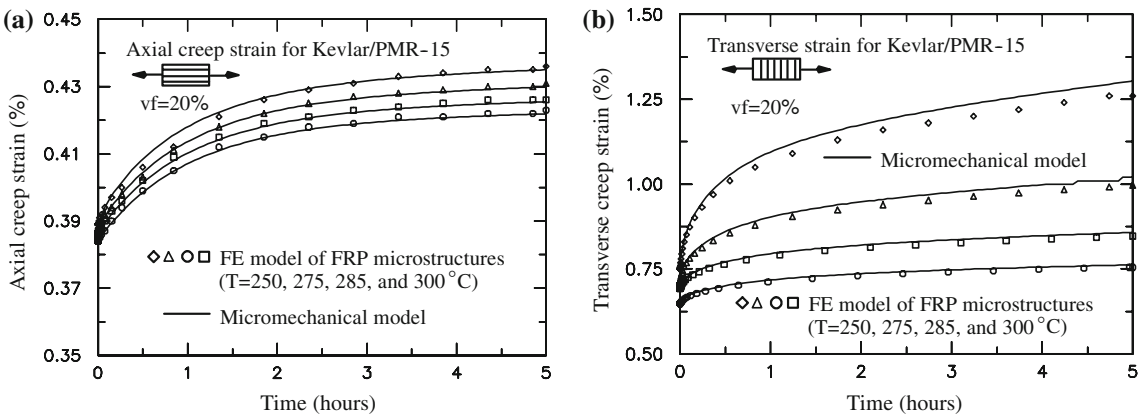

Fig. 10 Axial and transverse creep compliances of KFRP/PMR-15 composites at volume fraction 20% and $T = 250$, 275, 285, and 300°C

A finite element model of the detailed FRP microstructures, shown in Fig. 5, is used to simulate creep responses of the Kevlar/PMR-15 composites having 20% fiber volume fraction at various temperatures. The viscoelastic properties of the Kevlar fiber are assumed independent of temperatures, while the temperature dependent viscoelastic properties of PMR-15 are taken from [20]. The purpose is to verify the capability of the concurrent micromodel in predicting effective thermo-viscoelastic responses of Kevlar/PMR-15 composites. Figure 10 shows micromodel predictions of the thermo-viscoelastic responses of Kevlar/PMR-15 composites in the axial and transverse fiber directions. The responses from the concurrent micromodel are comparable to the ones obtained from the detailed FE microstructures.

5 Conclusion

A concurrent micromechanical model is formulated for predicting effective responses of FRP composites, whose fiber and matrix constituents exhibit different thermo-viscoelastic behaviors. The viscoelastic material properties for the fiber and matrix are allowed to change with the temperature field. An orthotropic thermo-viscoelastic constitutive model is used for the unidirectional fiber. This constitutive model is simplified for isotropic materials and used for the polymer matrix. The micromodel relations have been verified using limited experimental data on the thermo-elastic properties of graphite fiber/PMR-15 epoxy and the viscoelastic responses of Kevlar/epoxy. Detailed FE models of the FRP microstructures with different fiber volume fractions have been generated to verify the thermo-viscoelastic responses of the Kevlar/PMR-15 composites. Overall, good response predictions are observed. It is also found that the effects of fiber interactions on the overall composite responses are significant for composites with high fiber volume fractions subject to the transverse loads.

Acknowledgments This research is sponsored by the National Science Foundation through the Civil and Mechanical Systems (CMS) Division, under Grant No. 0546528.

Appendix A

This appendix describes a micromechanical relation of a unidirectional composite layer. This was previously introduced by Haj-Ali and Muliana [11] and Muliana and Haj-Ali [24] for analyzing stress–time-dependent responses on FRP composite materials and structures. The unit cell of the FRP (Fig. 1) is composed of four subcells. The first subcell is fiber constituent, while subcells 2, 3 and 4 represent the matrix constituents. The micromodel relations in the axial (fiber) direction are:

$$\begin{aligned} \Delta\varepsilon_{11}^{(1)} = \Delta\varepsilon_{11}^{(2)} = \Delta\varepsilon_{11}^{(3)} = \Delta\varepsilon_{11}^{(4)} = \Delta\overline{\varepsilon}_{11}, \\ V_1\Delta\sigma_{11}^{(1)} + V_2\Delta\sigma_{11}^{(2)} + V_3\Delta\sigma_{11}^{(3)} + V_4\Delta\sigma_{11}^{(4)} = \Delta\overline{\sigma}_{11}. \end{aligned} \tag{A.1}$$

Along the interfaces between the subcells with normal in the x_2-direction, the following relations should be fulfilled:

$$\begin{aligned} \Delta\sigma_{22}^{(1)} = \Delta\sigma_{22}^{(2)}, \\ \Delta\sigma_{22}^{(3)} = \Delta\sigma_{22}^{(4)}, \\ \tfrac{V_1}{V_1+V_2}\Delta\varepsilon_{22}^{(1)} + \tfrac{V_2}{V_1+V_2}\Delta\varepsilon_{22}^{(2)} = \Delta\overline{\varepsilon}_{22}, \\ \tfrac{V_3}{V_3+V_4}\Delta\varepsilon_{22}^{(3)} + \tfrac{V_4}{V_3+V_4}\Delta\varepsilon_{22}^{(4)} = \Delta\overline{\varepsilon}_{22}, \end{aligned} \tag{A.2}$$

$$\begin{aligned} \Delta\tau_{12}^{(1)} = \Delta\tau_{12}^{(2)}, \\ \Delta\tau_{12}^{(3)} = \Delta\tau_{12}^{(4)}, \\ \tfrac{V_1}{V_1+V_2}\Delta\gamma_{12}^{(1)} + \tfrac{V_2}{V_1+V_2}\Delta\gamma_{12}^{(2)} = \Delta\overline{\gamma}_{12}, \\ \tfrac{V_3}{V_3+V_4}\Delta\gamma_{12}^{(3)} + \tfrac{V_4}{V_3+V_4}\Delta\gamma_{12}^{(4)} = \Delta\overline{\gamma}_{12}. \end{aligned} \tag{A.3}$$

Considering interfaces between subcells with normal in the x_3-direction, the micromodel relations are expressed as:

$$\begin{aligned} \Delta\sigma_{33}^{(1)} = \Delta\sigma_{33}^{(3)}, \\ \Delta\sigma_{33}^{(2)} = \Delta\sigma_{33}^{(4)}, \\ \tfrac{V_1}{V_1+V_3}\Delta\varepsilon_{33}^{(1)} + \tfrac{V_3}{V_1+V_3}\Delta\varepsilon_{33}^{(3)} = \Delta\overline{\varepsilon}_{33}, \\ \tfrac{V_2}{V_2+V_4}\Delta\varepsilon_{33}^{(2)} + \tfrac{V_4}{V_2+V_4}\Delta\varepsilon_{33}^{(4)} = \Delta\overline{\varepsilon}_{33}, \end{aligned} \tag{A.4}$$

$$\begin{aligned}
\Delta\tau_{13}^{(1)} &= \Delta\tau_{12}^{(3)},\\
\Delta\tau_{13}^{(2)} &= \Delta\tau_{13}^{(4)},\\
\tfrac{V_1}{V_1+V_3}\Delta\gamma_{13}^{(1)} + \tfrac{V_3}{V_1+V_3}\Delta\gamma_{13}^{(3)} &= \Delta\overline{\gamma}_{13},\\
\tfrac{V_2}{V_2+V_4}\Delta\gamma_{13}^{(2)} + \tfrac{V_4}{V_2+V_4}\Delta\gamma_{13}^{(4)} &= \Delta\overline{\gamma}_{13}.
\end{aligned} \tag{A.5}$$

Finally, the transverse shear relations are summarized as:

$$\begin{aligned}
\Delta\tau_{23}^{(1)} = \Delta\tau_{23}^{(2)} = \Delta\tau_{23}^{(3)} = \Delta\tau_{23}^{(4)} &= \Delta\overline{\tau}_{23},\\
V_1\Delta\gamma_{23}^{(1)} + V_2\Delta\gamma_{23}^{(2)} + V_3\Delta\gamma_{23}^{(3)} + V_4\Delta\gamma_{23}^{(4)} &= \Delta\overline{\gamma}_{23}.
\end{aligned} \tag{A.6}$$

Appendix B

The nonzero components of the matrices $\boldsymbol{A}_1$ are:

$$\begin{aligned}
&\boldsymbol{A}_1(1,1) = \boldsymbol{A}_1(2,7) = \boldsymbol{A}_1(3,13) = \boldsymbol{A}_1(4,19) = 1,\\
&\boldsymbol{A}_1(5,2) = \boldsymbol{A}_1(9,4) = \frac{V^{(1)}}{V^{(1)}+V^{(2)}}, \qquad \boldsymbol{A}_1(5,8) = \boldsymbol{A}_1(9,10) = \frac{V^{(2)}}{V^{(1)}+V^{(2)}},\\
&\boldsymbol{A}_1(6,14) = \boldsymbol{A}_1(10,16) = \frac{V^{(3)}}{V^{(3)}+V^{(4)}}, \quad \boldsymbol{A}_1(6,20) = \boldsymbol{A}_1(10,22) = \frac{V^{(3)}}{V^{(3)}+V^{(4)}},\\
&\boldsymbol{A}_1(7,3) = \boldsymbol{A}_1(11,5) = \frac{V^{(1)}}{V^{(1)}+V^{(3)}}, \qquad \boldsymbol{A}_1(7,15) = \boldsymbol{A}_1(11,17) = \frac{V^{(3)}}{V^{(1)}+V^{(3)}},\\
&\boldsymbol{A}_1(8,9) = \boldsymbol{A}_1(12,11) = \frac{V^{(2)}}{V^{(2)}+V^{(4)}}, \qquad \boldsymbol{A}_1(8,21) = \boldsymbol{A}_1(12,23) = \frac{V^{(4)}}{V^{(2)}+V^{(4)}},\\
&\boldsymbol{A}_1(13,6) = V^{(1)} \quad \boldsymbol{A}_1(13,12) = V^{(2)}, \qquad \boldsymbol{A}_1(13,18) = V^{(3)} \quad \boldsymbol{A}_1(13,24) = V^{(4)}.
\end{aligned} \tag{B.1}$$

The nonzero components of the matrices $\boldsymbol{A}_2$ are:

$$\begin{aligned}
&\boldsymbol{A}_2(1,1) = C_{2211}^{(1)}, \quad \boldsymbol{A}_2(1,2) = C_{2222}^{(1)}, \quad \boldsymbol{A}_2(1,3) = C_{2233}^{(1)},\\
&\boldsymbol{A}_2(1,7) = -C_{2211}^{(2)}, \quad \boldsymbol{A}_2(1,8) = -C_{2222}^{(2)}, \quad \boldsymbol{A}_2(1,9) = -C_{2233}^{(2)},\\
&\boldsymbol{A}_2(2,13) = C_{2211}^{(3)}, \quad \boldsymbol{A}_2(2,14) = C_{2222}^{(3)}, \quad \boldsymbol{A}_2(2,15) = C_{2233}^{(3)},\\
&\boldsymbol{A}_2(2,19) = C_{2211}^{(4)}, \quad \boldsymbol{A}_2(2,20) = C_{2222}^{(4)}, \quad \boldsymbol{A}_2(2,21) = C_{2233}^{(4)},\\
&\boldsymbol{A}_2(3,4) = C_{1212}^{(1)}, \quad \boldsymbol{A}_2(3,10) = -C_{1212}^{(1)}, \quad \boldsymbol{A}_2(4,16) = C_{1212}^{(3)}, \quad \boldsymbol{A}_2(4,22) = -C_{1212}^{(4)},\\
&\boldsymbol{A}_2(5,1) = C_{3311}^{(1)}, \quad \boldsymbol{A}_2(5,2) = C_{3322}^{(1)}, \quad \boldsymbol{A}_2(5,3) = C_{3333}^{(1)},\\
&\boldsymbol{A}_2(5,13) = -C_{3311}^{(3)}, \quad \boldsymbol{A}_2(5,14) = C_{3322}^{(3)}, \quad \boldsymbol{A}_2(5,15) = C_{3333}^{(3)},\\
&\boldsymbol{A}_2(6,7) = C_{3311}^{(2)}, \quad \boldsymbol{A}_2(6,8) = C_{3322}^{(2)}, \quad \boldsymbol{A}_2(6,9) = C_{3333}^{(2)},\\
&\boldsymbol{A}_2(6,19) = -C_{3311}^{(4)}, \quad \boldsymbol{A}_2(6,20) = -C_{3322}^{(4)}, \quad \boldsymbol{A}_2(6,21) = -C_{3333}^{(4)},\\
&\boldsymbol{A}_2(7,5) = C_{1313}^{(1)}, \quad \boldsymbol{A}_2(7,17) = -C_{1313}^{(3)}, \quad \boldsymbol{A}_2(8,11) = C_{1313}^{(2)}, \quad \boldsymbol{A}_2(8,23) = -C_{1312}^{(4)},\\
&\boldsymbol{A}_2(9,6) = \boldsymbol{A}_2(10,6) = \boldsymbol{A}_2(11,6) = C_{2323}^{(1)},\\
&\boldsymbol{A}_2(9,12) = -C_{2323}^{(2)}, \quad \boldsymbol{A}_2(10,18) = -C_{2323}^{(3)}, \quad \boldsymbol{A}_2(11,24) = -C_{2323}^{(4)}.
\end{aligned} \tag{B.2}$$

The nonzero components of the matrices $\boldsymbol{D}_1$ are:

$$\begin{aligned}
&\boldsymbol{D}_1(1,1) = \boldsymbol{D}_1(2,1) = \boldsymbol{D}_1(3,1) = \boldsymbol{D}_1(4,1) = 1,\\
&\boldsymbol{D}_1(5,2) = \boldsymbol{D}_1(6,2) = \boldsymbol{D}_1(7,3) = \boldsymbol{D}_1(8,4) = 1,\\
&\boldsymbol{D}_1(9,4) = \boldsymbol{D}_1(10,4) = \boldsymbol{D}_1(11,5) = \boldsymbol{D}_1(12,5) = \boldsymbol{D}_1(13,6) = 1.
\end{aligned} \tag{B.3}$$

References

1. Aboudi, J.: Mech. of Composite Materials: a Unified Micromechanical Approach. Elsevier, Amsterdam (1991)
2. Alwis, K.G.N., Burgoyne, C.J.: Time–temperature superposition to determine the stress-rupture of aramid fibers. Appl. Compos. Mater. **13**, 249–264 (2006)
3. Antonakakis, J.N., Bhargava, P., Chuang, K.C., Zehnder, A.T.: Linear viscoelastic properties of HFPE-II-52 polyimide. J. Appl. Pol. Sci. **100**, 3255–3263 (2006)
4. Benedikt, B., Rupnowski, P., Kumosa, M.: Viscoelastic stress distribution and elastic properties in unidirectional composites with large volume fractions of fibers. Acta Mater. **51**, 3483–3493 (2003)
5. Brinson, L.C., Knauss, W.G.: Thermo-rheologically complex behavior of multiphase viscoelastic materials. J. Mech. Phys. Solids **39**(7), 859–880 (1991)
6. Caruthers, J.M., Adolf, D.B., Chambers, R.S., Shrikhande, P.: A thermodynamically consistent, nonlinear viscoelastic approach for modeling glassy polymers. Polymer **45**, 4577–4597 (2004)
7. Christensen, R.M.: Mechanics of Composite Materials. Dover Publications, New York (2005)
8. Haddad, Y.M., Tanari, S.: On the micromechanical characterization of the creep response of a class of composite systems. J. Press. Vessel Technol. Trans. ASME, **111**(2), 177–182 (1989)
9. Haftchenari, H., Al-Salehi, F.A.R., Al-Hasani, S.T.S., Hinton, M.J.: Effect of the temperatures on the tensile strength and failure modes of angle ply aramid fiber (KRP) tube under hoop loading. Appl. Compos. Mater. **9**, 99–115 (2002)
10. Haj-Ali, R.M., Muliana, A.H.: Numerical finite element formulation of the schapery nonlinear viscoelastic material model. Int. J. Numer. Method Eng. **59** (2004)
11. Haj-Ali, R.M., Muliana, A.H.: A multi-scale constitutive framework for the nonlinear analysis of laminated composite materials and structures. Int. J. Solids Struct. **41**, 3461–3490 (2004)
12. Hanson, M.P.: Feasibility of Kevlar 49/PMR-15 polyimide for high temperature applications. In: 12th National SAMPE Technical Conference, pp. 1–15. 7–9 October (1980)
13. Harris, C.E., Gates, T.S. (eds.): High Temperature and Environmental Effects on Polymeric Composites. ASTM, Philadelphia, ASTM STP Paper No. 1174 (1993)
14. Harper, B.D., Weitsman, Y.: Characterization method for a class of thermorheologically complex materials. J. Rheol. **29**, 49–66 (1985)
15. Hashin, Z., Humprey, E. A., Goering, J.: Analysis of thermoviscoelastic behavior of unidirectional fiber composites. Composites Sci. Technol. **29**, 103–131 (1987)
16. Knauss, W.G., Emri, I.: Volume change and the nonlinearly thermoviscoelastic constitution of polymers. Pol. Eng. Sci. **27**, 86–100 (1987)
17. Li, J., Weng, G.J.: Stress–strain relations of a viscoelastic composite reinforced with elliptic cylinders. J. Thermoplast. Compos. Mater. **10**, 19–30 (1997)
18. Li, J., Weng, G.J.: Influence of inclusion microgeometry on some thermomechanical properties of isotropic polymer-matrix composites. J. Eng. Mater. Technol. Trans. ASME **119**(3), 242–250 (1997)
19. Lou, Y.C., Schapery, R.A.: Viscoelastic characterization of a nonlinear fiber-reinforced plastic. J. Compos. Mater. **5**, 208–234 (1971)
20. Marias, C., Villoutreix, G.: Analysis and modeling of the creep behavior of the thermostable PMR-15 polyimide. J. Appl. Polym. Sci. **69**, 1983–1991 (1998)
21. Morgan, R.J., Shih, E.E., Lincoln, J.E.: Thermal Properties of High Temperature Polymer Matrix Fibrous Composites. Handbook of Thermal Analysis and Calorimetry, vol. 3. In: Cheng, S.Z.D. (ed.) Elsevier Sci, Amsterdam (2002)
22. Morland, L.W., Lee, E.H.: Stress analysis for linear viscoelastic materials with temparature variations. Soc. Rheol. Trans. **4**, 233–263 (1960)
23. Muliana, A.H.: Integrated micromechanical-structural framework for the nonlinear viscoelastic behavior of laminated and pultruded composite materials and structures. Ph.D. Thesis, Georgia Institute of Technology (2004)
24. Muliana, A.H., Haj-Ali, R.M.: Nested nonlinear viscoelastic and micromechanical models for the analysis of pultruded composite structures. Mech. Mater. (MOM) J. **36**, 1087–1110 (2004)
25. Muliana, A.H., Haj-Ali, R.M.: Analyses for creep behavior and collapse of FRP composite structures. Compos. Struct. **73**(3), 331–341 (2006)
26. Muliana, A.H., Haj-Ali, R.M.: Multi-scale modeling for the long-term behavior of FRP composite structures. AIAA J. **43**(8), 1815–1822 (2005)
27. Muliana, A.H., Nair, A., Khan, K.A., Wagner, S.: Characterization of thermo-mechanical viscoelastic and long-term behaviors of multi-layered composite materials. Compos. Sci. Tech. **66**, 2907–2924 (2006)
28. Muliana, A.H., Kim, J.S.: A concurrent micromechanical model for nonlinear viscoelastic behaviors of composites reinforced with solid spherical particles. Int. J. Solids Struct. **44**, 6891–6913 (2007)
29. Muliana, A.H., Khan, K.A.: A time integration algorithm for thermo-rheologically complex polymers. Comput. Mater. Sci. **41**, 576–588 (2008)
30. Muliana, A.H.: Multi-scale framework for the thermo-viscoelastic analyses of polymer composites. Mech. Res. Commun. **34**, 561–567 (2007)
31. Muliana, A.H., Haj-Ali, R.: A multi-scale framework for the thermo-rheologically complex multi-layered composites. Int. J. Solids Struct. **45**, 2937–2963 (2008)
32. Nemat-Nasser, S., Hori, M.: Micromechanics: Overall Props. of Heterogeneous Materials. Elsevier, Amsterdam (1999)
33. Odegard, G., Kumosa, M.: Elastic-plastic and failure properties of a unidirectional graphite/PMR-15 composites at room and elevated temperature. Comput. Sci. Tech. **60**, 2979–2988 (2000)
34. Peretz, D., Weitsman, Y.: The nonlinear thermoviscoelastic characterizations of FM-73 adhesive. J. Rheol. **27**(2), 97–114 (1983)
35. Rupnowski, P., Gentz, M., Kumosa, M.: Mechanical response of a unidirectional graphite fiber/polyimide composite as a function of temperature. Compos. Sci. Tech. **66**, 1045–1055 (2006)

36. Sadkin, Y., Aboudi, J.: Viscoelastic behavior of thermo-rheologically complex resin matrix composites. Compos. Sci. Tech. **36**, 351–365 (1989)
37. Sawant, S., Muliana, A.: A thermo-mechanical viscoelastic analysis of orthotropic media. Compos. Struct. **83**, 61–72 (2008)
38. Schapery, R.A.: On the characterization of nonlinear viscoelastic materials. Polym. Eng. Sci. **9**(4), 295–310 (1969)
39. Struik, L.C.E.: Physical aging in amorphous polymers and other materials. Elsevier Scientific Publishing Company, New York (1978)
40. Tschoegl, N.W., Knauss, W.G., Emri, I.: The effect of temperature and pressure on the mechanical properties of thermo and/or piezorheologically simple polymeric materials in thermodynamics equilibrium: a critical review. Mech. Time Dept. Matr. **6**, 53–99 (2002)
41. Walruth, D.E.: Viscoelastic response of a unidirectional composite containing two viscoelastic constituents. Exper. Mechan. **31**(2), 111–117 (1991)
42. Walton, P.L., Majumdar, A.J.: Creep of Kevlar 49 fibre and a Kevlar 49-cement composite. J. Mater. Sci. **18**, 2939–2946 (1983)
43. Wang, J.Z., Dillard, D.A., Ward, T.C.: Temperature and stress effects in the creep of aramid fibers under transient moisture conditions and discussions on the mechanisms. J. Polym. Sci. Part B **30**, 1391–1400 (1992)
44. Wang, J.Z., Dillard, D.A.: Testing of viscoelasticity of single fibers under transient moisture conditions. Exper. Tech. **15**(5), 47–49 (1991)
45. White, S.R., Hartman, A.B.: Effect of cure state on stress relaxation in 3501–6 epoxy resin. J. Eng. Mater. Technol. Trans. ASME **119**(3), 262–265 (1997)
46. Wineman, A., Rajagopal, K.R.: Mech Responses of Polymers, an Intro. Cambridge Univ. Press, London (2000)
47. Zheng, S.F., Weng, G.J.: A new constitutive equation for the long-term creep of polymers based on physical aging. Eur. J. Mechan. A Solids **21**, 411–421 (2002)